WILEY | Hindawi

Research Article

Experimental Study on the Pore Structure of Middle- and Low-Rank Coal and Its Influence on Methane Adsorption

Gaini Jia [ID],[1] **Ming Yang** [ID],[1,2,3] **Xuebo Zhang** [ID],[1,2,3] **and Lei Liu** [ID][4]

[1]*School of Safety Science and Engineering, Henan Polytechnic University, Jiaozuo 454003, China*
[2]*State Collaborative Innovation Center of Coal Work Safety and Clean-Efficiency Utilization, Henan Polytechnic University, Jiaozuo 454003, China*
[3]*State Key Laboratory Cultivation Base for Gas Geology and Gas Control, Henan Polytechnic University, Jiaozuo 454003, China*
[4]*School of Resources and Safety Engineering, Chongqing University, Chongqing 400044, China*

Correspondence should be addressed to Ming Yang; yming@hpu.edu.cn

The pore characteristics of coal have an important influence on the coal adsorption of methane. The liquid nitrogen adsorption method was used to study the pore structure of low- and middle-rank coal samples from two aspects: pore specific surface area and pore shape. Low-field nuclear magnetic resonance (NMR) technology was used to study the difference in methane adsorption of coal samples under the same adsorption conditions. The influence and mechanism of the pore structure of middle- and low-rank coal samples on gas adsorption are discussed and analyzed. The results show the following: (1) There are differences in the adsorption capacity of medium- and low-rank coal samples. Within 1 h of methane inflation, the methane adsorption capacity of middle-rank coals such as Henan Pingdingshan (PDS) and Shanxi Wangzhuang (WZ) and Xinjiang low-rank coals (XJ) increases by 36.4%, 31.7%, and 35.8%, respectively, and as the inflation time is extended to the cumulative inflation of 10 h, the order of the increase in methane adsorption capacity is still PDS>XJ>WZ. (2) The pore types of the experimental coal samples are mostly wedge-shaped pores and ink bottle-shaped pores. The order of the BET specific surface area of the coal samples is in the order of WZ>PDS> XJ, which means that the WZ samples can provide more adsorption sites for gas molecule adsorption, but under the same adsorption conditions, the WZ sample has the least amount of gas adsorbed. Further analysis shows that the order of the tortuosity of the coal sample is WZ>XJ>PDS, which means that the WZ sample has a large pore tortuosity, a long channel for methane molecules to diffuse into the internal pores of the coal sample, and large diffusion resistance. It is the main reason why the methane adsorption capacity of WZ coal samples is less than that of PDS and XJ coal samples in the same adsorption conditions.

1. Introduction

Gas is an associated organism in the coal formation process. Gas mainly exists in the coal in an adsorbed state, and the gas adsorption by coal is related to the coal pore structure. Therefore, the coal pore and fissure system provides a place for gas storage and transportation. At the same time, it also provides a place for the storage and migration of coal methane [1]. Under a certain methane pressure, the adsorption of coal to methane is the same as the flow of coal seam methane. In the process of coal adsorption of methane, methane gas molecules enter the coal body under the action of the pressure gradient or under the action of the concentration difference [2]. Methane adsorption mainly occurs in micropores and is affected by the methane concentration gradient and pore structure. The study of coal pore heterogeneity is beneficial to the exploration and development of coalbed methane [3]. Previous scholars have studied the adsorption capacity of coal and the factors affecting the adsorption capacity of coal. Related studies believe that coal methane adsorption, desorption, diffusion, and coal pore structure are closely related. Sun [4] found that the pore structure of different ranks affects the methane adsorption capacity of coal samples. Li [5] used mercury intrusion and liquid

nitrogen adsorption experiments to study the pore types and pore size distribution characteristics of low-rank coal; the experimental results show that the pore structure of low-rank coal affects the adsorption capacity of coal to gas. The adsorption balance of coal is destroyed by an external force, which can easily lead to gas accidents [6–10]. Jiang et al. [11] divided the pores of tectonic coal into four categories based on low-temperature liquid nitrogen adsorption (LNA) experiments. Li et al. [12] used SEM to observe the pore structure of different rank coals, which is consistent with the analysis results of LAN experiments. The types of coal mine accidents are gas, rockburst, flood, and roof accidents [7–10, 13]. Jiang et al. [14] found through fractal dimension analysis that the pores of low-rank coals are more complex than those of middle-rank coals. With the deepening of research, nondestructive low-field NMR technology is gradually used to study coal pore structure and coal gas adsorption process. Liquid nitrogen freeze-thaw has been used in oil, shale gas, and coalbed methane exploitation as an efficient fracturing technology; [15] studied the effect of different coal ranks and liquid nitrogen soaking times on the temperature distribution of coal samples. Qin et al. [16] studied the effect of liquid nitrogen freezing on the adsorption capacity of different rank coals. Low-field NMR technology can also be used to study the pore structure of coal, such as the type of pores and cracks, effective porosity, and pore structure distribution [17]. Chen et al. [18] also used this method to examine the gas adsorption capacity. Other scholars [19–21] also used this technology to obtain low-rank coals with the best development of adsorption pores, followed by seepage pores and fissures; middle-rank coals were mainly developed with micropores, large pores, or fissures. Mesopores are relatively underdeveloped, while high-rank coals are dominated by micropores, while mesopores, macropores, and cracks are relatively underdeveloped. Under the action of external load, coal is prone to brittle failure, which will also affect the coal gas adsorption balance [7, 10, 22, 23]. Tang et al. [24] and Yao et al. [25] used this technology to study the process of coal sample gas adsorption. Some experimental methods such as mercury injection (MIP), scanning electron microscopy (SEM), low-field NMR technology, and low-temperature LNA were used to study the vitrain and durain in low-rank coal [26]. The pore types of low-rank coal are complex, and it is necessary to use a combination of various detection methods to study its pore structure [27]. To sum up, the commonly used methods for the study of the coal pore structure include the MIP method, low-temperature LNA method, and low-field NMR technology. Scholars have carried out a lot of research on the pore structure of low- and middle-rank coals and the differences and influencing factors of gas adsorption, but there is no unified understanding of the influence and control mechanism of the difference of the micropore structure of middle- and low-rank coal on the gas adsorption process; further research is needed. Therefore, this paper takes low- and middle-rank coal as an example, studies the difference of the micropore structure of low-rank and middle-rock coal by using low-temperature LNA, carries out experiments on coal gas adsorption under the same adsorption conditions with

TABLE 1: Industrial analysis for experimental coal samples.

Coal	a (cm³·t⁻¹)	b (MPa⁻¹)	V_{daf} (%)	A_{ad} (%)	V_{daf} (%)	$R_{0,m}$ (%)
PDS	26.954	1.098	0.63	8.89	13.49	1.83
WZ	20.661	1.110	0.96	12.41	31.92	1.15
XJ	24.155	0.825	1.02	7.33	40.25	0.79

the help of nondestructive and dynamic detection low-field NMR technology, and analyzes the control mechanism and influence of the pore structure on the difference of gas adsorption process of experimental coal samples analyzed.

2. Sample Preparation and Testing

2.1. Coal Sample Collection. The coal samples were from Shanxi Wangzhuang, Henan Pingdingshan, and Xinjiang Aiweiergou. The experimental coal samples were all taken from newly mined large fresh coal samples. Among them, some processing plants are 3 mm~6 mm, 60 mesh~80 mesh granular, which are, respectively, used for LNA adsorption experiments and industrial analysis. Some coal samples were processed into cylindrical coal samples with $\varphi 25 \times 50$ mm for gas adsorption NMR experiments. Table 1 shows the industrial analysis results of the experimental coal samples.

Vitrinite reflectance reflects the degree of coal metamorphism. Traditionally, the U.S. CBM industry defines low-rank coal as $R_{0,m}$ less than 0.7% or 0.8%. The test results of XJ coal samples are below 0.8%; based on $R_{0,m}$ and high volatility, XJ coal samples are low-rank coal [14, 28]. $R_{0,m}$ of WZ and PDS coal samples are between 1.0% and 1.5%, which is medium-rank coal [5].

2.2. Basic Principles of NMR. Low-field NMR technology is based on the principle of directional arrangement of hydrogen nuclei under the action of an external magnetic field. By measuring the relaxation characteristics of hydrogen nuclei fluids (H_2O, CH_4) in coal pores, the pore structure and pore size distribution characteristics of coal are studied. NMR experiments are used to study coal rock pores and cracks, mainly to obtain the relationship between NMR intensity and transverse relaxation time (T_2), so as to obtain the pore structure distribution of coal samples. The principle of NMR T_2 [29, 30] is

$$\frac{1}{T_2} \approx F_S \frac{\rho}{r} = \rho \frac{S}{V}. \tag{1}$$

In formula (1), ρ is the surface relaxation rate, F_S is the pore shape factor (tubular pores and plate pores, $F_S = 2$), r is the pore radius, and S/V is the pore specific surface area of the coal sample.

In formula (1), the pore radius of coal is related to T_2; that is, the larger the T_2, the larger the pore radius. Therefore, different levels of pores and fractures can be divided according to the T_2 spectrum.
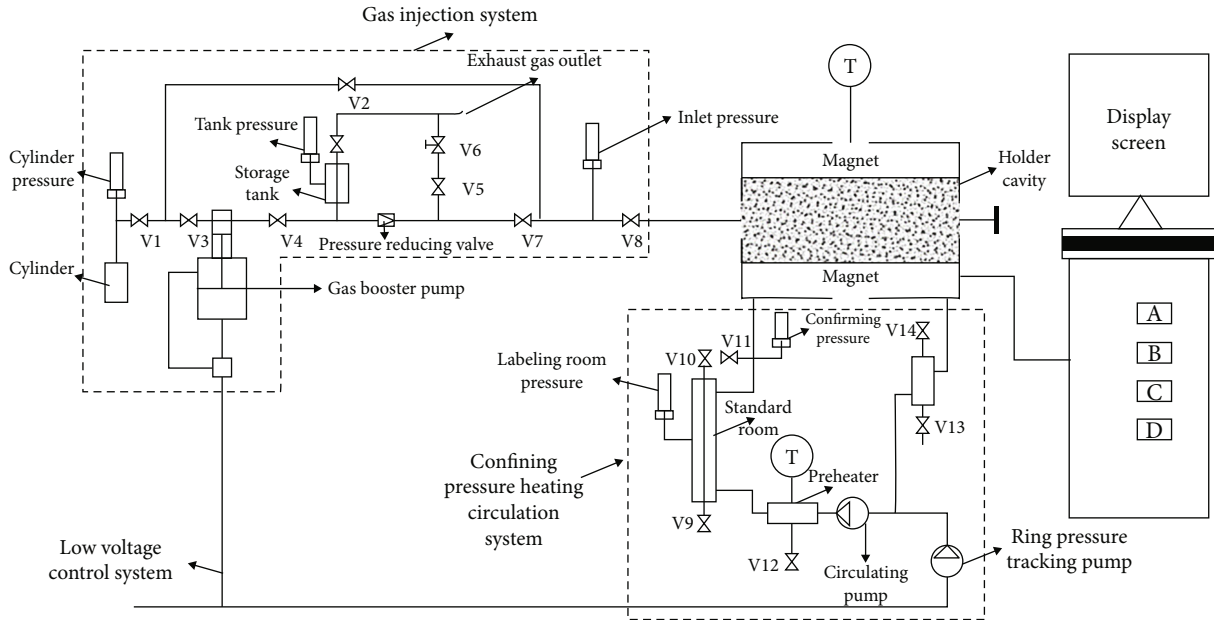
2.3. Test Equipment and Procedures

FIGURE 1: Schematic diagram of methane adsorption low-field nuclear magnetic resonance experimental system.

(1) The specific surface area of the coal sample was measured by a V-Sorb 2800TP specific surface area analyzer

(2) The gas adsorption experiment was performed using a low-field NMR instrument of the model MesoMR23-060H-I. The connection system diagram of the experimental coal sample gas adsorption experimental equipment is shown in Figure 1. In Figure 1, V1-V14 are valve control switches, A is the computer host, B is the temperature control unit, C is the radio frequency unit, and D is the gradient unit

First, the columnar raw coal samples were dried, the temperature was set to 60°C, and the drying time was 12 h, and then cooled to room temperature. Second, place the dry coal sample into the "holder cavity" in Figure 1. Third, all pipelines were connected, and fixed confining pressure 3 MPa is applied on the dried coal samples; vacuum the pipeline to ensure no air leakage. Finally, carry out NMR experiments on coal gas adsorption characteristics, the gas adsorption time of the experimental coal samples was 10 h, and the signal is collected once every 0.5 h, a total of 20 times.

2.4. Free-State Methane Calibration Experiment. In order to distinguish the T_2 relaxation time range corresponding to adsorbed methane and free methane, at first, the NMR T_2 spectral characteristics of free methane have been determined. Due to the incomplete sealing between the coal sample and the "holder cavity," when coal adsorbs methane, high-pressure methane will flow into the gap from the gas cylinder. This part of the methane is affected by the experimental conditions; therefore, the amount of methane contained in coal should not be included in this part of methane.
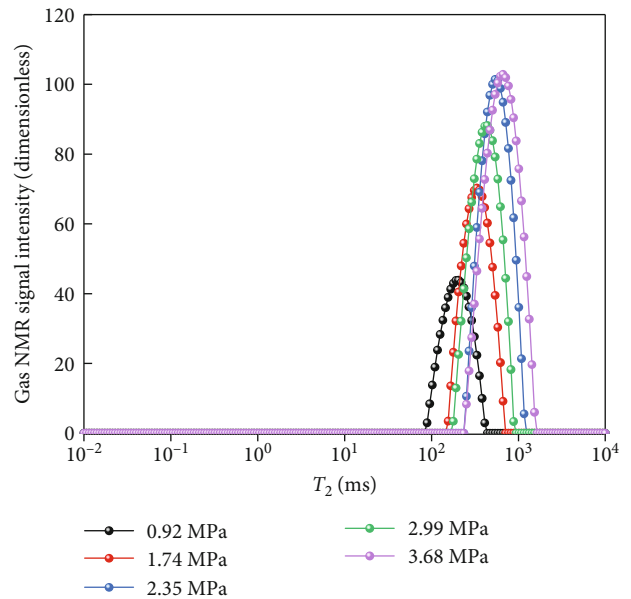

FIGURE 2: Free-state gas T_2 spectra at different inflation pressures.

In the experiment, the calibration experiment of free-state gas NMR T_2 spectra was carried out first, and then, the gas NMR experiment of the adsorption of medium- and low-rank coal was carried out. Previous research results show that the free-state gas amplitude integral and the T_2 both increase, and the free-state gas peak increases. The T_2 spectral curve has only one characteristic peak [24, 25, 31], which can further distinguish different states of methane. Figure 2 shows the T_2 spectra of free-state gas at different gas pressures.

It can be seen in Figure 2 that the free-state gas T_2 spectrum has a characteristic peak, and the T_2 ranges from 89.07 ms to 1534.37 ms. As the gas pressure increases, T_2
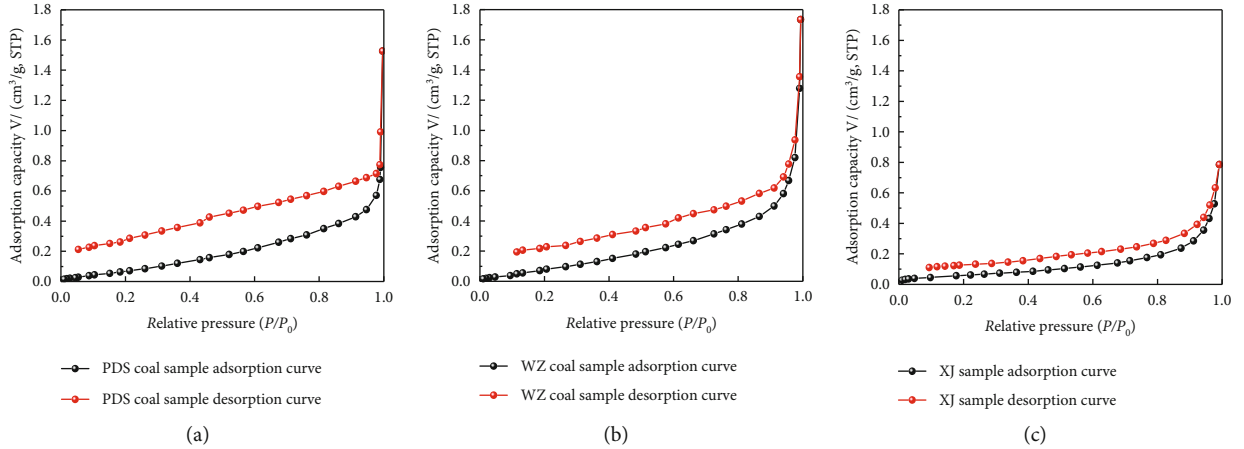
FIGURE 3: Experimental coal sample adsorption-desorption curve.

gradually shifts to the right; this is consistent with earlier findings [25, 31, 32].

3. Experimental Results

3.1. Experimental Coal Sample Liquid Nitrogen Adsorption Test Results. The experimental results of nitrogen adsorption and desorption of the experimental coal samples are shown in Figure 3.

In Figure 3, (1) with the increase of relative pressure, the nitrogen adsorption capacity of coal also increases accordingly. (2) Under the same adsorption conditions, the PDS coal sample has the strongest ability to adsorb nitrogen, WZ is the second, and XJ is the weakest. (3) By analyzing Figure 3, when $P/P_0 < 0.5$, the nitrogen adsorption of the experimental coal samples rose slowly. When $P/P_0 > 0.5$, the nitrogen adsorption of the experimental coal samples rose rapidly, indicating that a large amount of liquid nitrogen entered the pores of the experimental coal samples. Due to the different pressures required for liquid nitrogen adsorption and condensation and desorption and evaporation, the adsorption and desorption curves of the experimental coal samples do not overlap; that is, a hysteresis loop occurs. The shape of the hysteresis loop represents different pore shapes [33, 34]. (4) The desorption curves of PDS, WZ, and XJ coal samples only show a sudden drop when $P/P_0 > 0.5$; that is, the coal sample contains more medium and large pores. The pore types of the coal samples are mainly wedge-shaped pores.

Table 2 shows the test results of the pore specific surface area of the experimental coal samples. The pore size classification refers to the B.B. Hodot pore classification standard [35].

From the analysis of Table 2, it can be seen that the pore specific surface area of the experimental coal samples is distributed at each stage, of which micropores account for the largest proportion. The micropore specific surface area of medium-rank coal accounts for more than 60.0% of the total pore specific surface area; the pore specific surface area of low-rank coal is mainly concentrated in micropores and small pores.

TABLE 2: Test results of pore specific surface area by liquid nitrogen adsorption method.

Project		PDS	WZ	XJ
BET specific surface area (m²/g)		7.2	9.1	5.2
Area ratio of each aperture (%)	<10 nm	87.4	80.3	68.2
	10~100 nm	9.2	14.9	31.1
	>100 nm	3.4	4.8	0.7

3.2. Analysis of Experimental Results of Methane Adsorption on Coal Samples. The methane adsorption NMR experiments of the experimental coal samples were all at a constant confining pressure 3 MPa and constant gas pressure 0.74 MPa. Figure 4 shows the experimental results of gas adsorption NMR experiments on coal samples. From the T_2 spectrum of gas adsorption NMR, the change rule of the gas adsorption process of experimental coal samples can be seen more intuitively.

Yao et al. [17] classified coal sample pores into different types according to the NMR measurement results of coal samples. Generally, the NMR T_2 spectrum of coal samples is divided into the single peak, double peak, or triple peak. T_2 corresponding to the crack is >100 ms, T_2 corresponding to the seepage pores (large and medium pores, $0.1\,\mu m \sim 1\,\mu m$) is between 20 and 50 ms, and T_2 corresponding to the adsorption pores ($<0.1\,\mu m$) is 0.5~2.5 ms. In Figure 4, the experimental coal sample NMR T_2 spectrum has three peaks at $T_2 < 1.83$ ms, $T_2 = 1.83~89.07$ ms, and $T_2 = 178.373~766.341$ ms.

Combined with the experimental results of coal sample free-state gas calibration in Figure 2, the third peak ($T_2 = 89.07~1534.37$ ms) in Figure 4 is a free-state gas spectrum. It can be seen from equation (1) that the coal sample pores are proportional to the transverse relaxation time T_2, so T_2 of medium and large pores is larger than that of micropores. Therefore, $T_2 < 1.83$ ms in Figure 4 corresponds to the adsorbed methane in the micropores, and $T_2 = 1.83~89.07$ ms corresponds to the free methane contained in coal [25, 32].

In Figure 4, under the same adsorption conditions, we can find that the morphological distribution of the T_2 spectrum in
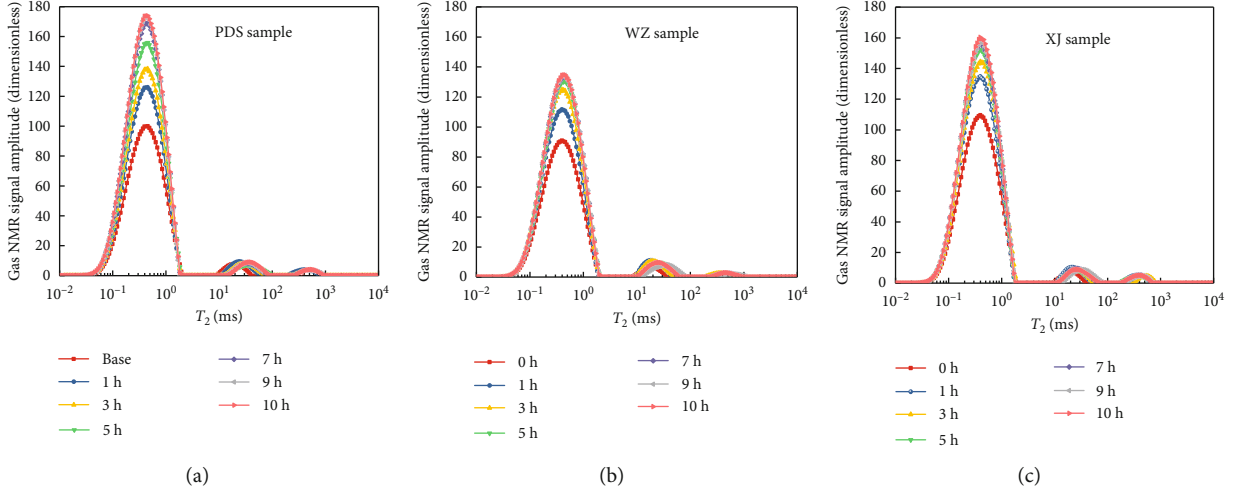
Figure 4: T_2 spectrum curves of experimental coal sample gas in the adsorption process.

different coal samples is similar; that is, the T_2 spectrum of the experimental coal samples has three separate peaks, and with the increase of the aeration time, the area of different peaks increases at different speeds, but the general trend of the T_2 spectrum changes. With the increase of inflation time, it first increased rapidly and then increased slowly.

Different from experimental coal samples in the gas adsorption process, the gas adsorption T_2 spectrum of the PDS coal sample increased rapidly within 0~7 h, and then, the change trend of the T_2 spectrum was not obvious with the increase of the gas charging time (Figure 4(a)). For the gas of the WZ and XJ coal samples, the adsorption T_2 spectrum increased rapidly within 0~5 h. This may be related to the adsorption mechanism between methane gas molecules and coal pore surfaces. The adsorption conditions are the same, the order of gas adsorption capacity of the experimental coal samples is as follows: PDS>XJ>WZ, and there may be many interconnected pores in the micropores of PDS coal samples, which are beneficial to the adsorption of methane molecules by coal.

3.2.1. The Amount of Adsorbed Methane Changes with the Inflation Time. The adsorption amount of methane gas molecules in coal micropores is expressed by the integral of the amplitude of the T_2 spectrum curve of the adsorbed gas. The relationship between inflation time and integrated amplitude of adsorbed methane is shown in Figure 5.

The fitting curves are

$$\text{PDS sample}: S_{\text{Adsorbed methane}} = \frac{1209.8t}{1 + 0.44t} \left(R^2 = 0.99\right),$$

$$\text{WZ sample}: S_{\text{Adsorbed methane}} = \frac{508.2t}{1 + 0.32t} \left(R^2 = 0.99\right),$$

$$\text{XJ sample}: S_{\text{Adsorbed methane}} = \frac{831.6t}{1 + 0.44t} \left(R^2 = 0.99\right).$$

$$(2)$$

By analyzing Figure 5, the amount of methane adsorbed by the coal samples in different experiments first increases
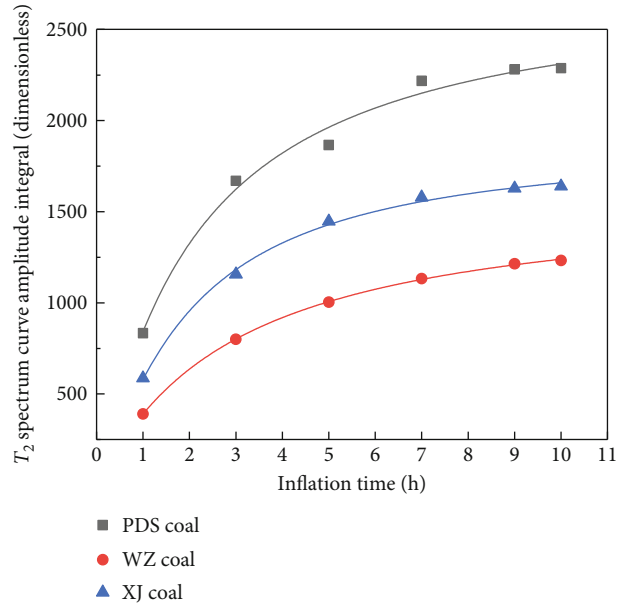

Figure 5: Variation of the integrated gas amplitude in the adsorbed state with the charging time.

rapidly with the aeration time and then increases slowly. When aerated for 1 h, the amount of methane adsorbed by PDS, WZ, XJ, and other coal samples increased by 36.4%, 31.7%, and 35.8%, respectively, indicating that the initial adsorption speed of PDS coal samples is faster. When aerated for 3 h, the adsorption amount of PDS, WZ, and XJ coal samples increased by 73.0%, 64.9%, and 70.6%, respectively. The adsorption rate of the experimental coal sample was faster at the initial gas filling (1~3 h); it is difficult for coal samples to adsorb gas in a short time to reach the adsorption equilibrium, which was related to the properties of coal and gas diffusion characteristics. The adsorbed methane amount of PDS, WZ, and XJ coal samples increased by 97.0%, 91.9%, and 96.3%, respectively, indicating that the methane adsorption capacity of coal samples such as PDS and XJ increased faster than that of WZ coal samples.

It takes a long time for coal sample gas adsorption equilibrium [36]. In this experiment, the coal samples were adsorbed for 10 h, and they did not reach adsorption equilibrium. In Figure 5, according to the fitting results, the amount of gas adsorbed by the coal sample is in accordance with the relationship between the aeration time: $s_{\text{Adsorbed methane}} = abt^c/1 + bt^c$ (a, b, and c are coefficients, $R^2 \geq 0.9$). It shows that this mathematical model can be used to describe the change process of the amount of adsorbed gas in the columnar coal sample with the aeration time.

3.2.2. The amount of free methane changes with the inflation time. Larger pores in coal provide channels for the migration of free gas; the integral of the free gas T_2 spectrum curve amplitude represents the amount of free gas contained in the coal sample. Figure 6 is a graph showing the relationship between the integral of the free-state gas amplitude and the charging time.

The fitting curves are

$$\text{PDS sample} : S_{\text{Free methane}} = \frac{241.2t^{0.58}}{1 + 1.29t} \left(R^2 = 0.98\right),$$

$$\text{WZ sample} : S_{\text{Free methane}} = \frac{58.1t^{0.81}}{1 + 0.01t} \left(R^2 = 0.92\right), \qquad (3)$$

$$\text{XJ sample} : S_{\text{Free methane}} = \frac{203.9t^{0.62}}{1 + 1.03t} \left(R^2 = 0.99\right).$$

In Figure 6, it can be seen that the free methane content of different coal samples under the same adsorption conditions varies with the aeration time. With aeration for 1 h, the free methane content of the PDS, WZ, and XJ coal samples increased by 68.2%, 65.8%, and 71.2%, respectively, indicating that the PDS coal sample contains more free methane than the Shanxi coal sample; 3 h after aeration, the free methane content of the PDS, WZ, and XJ coal samples increased by 93.1%, 89.3%, and 96.0%, respectively, compared with the initial aeration, and for PDS after 7 h of aeration, the free methane content of coal samples of WZ and XJ increased by 96.7%, 92.7%, and 96.0%, respectively, indicating that the free methane content of coal samples such as PDS and XJ increased faster than that of WZ coal samples under the same adsorption conditions. This change corresponds to the amount of adsorbed methane change with inflation time.

Under the same adsorption conditions, the amount of free methane of the coal sample is in accordance with the relationship between the aeration time: $S_{\text{Free methane}} = a'b't^{c'}/1 + b't^{c'}$ (a', b', and c' are coefficients, $R^2 \geq 0.90$). It is also shown that the mathematical model is used to describe the variation of the free methane content in the cylindrical coal sample with the aeration time.

4. Analysis and Discussion

(1) The order of the amount of gas adsorbed by the experimental coal samples under the confining pressure of 3 MPa and the gas pressure of 0.74 MPa is PDS>XJ>WZ. From Table 1, the order of the
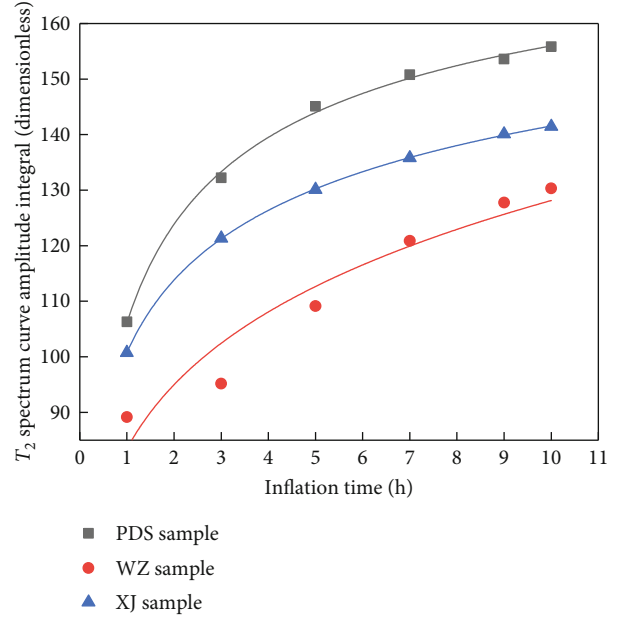

FIGURE 6: Relationship between inflation time and integrated amplitude of free methane.

adsorption constant "a" of the experimental coal sample is PDS>XJ>WZ. Because the adsorption constant "a" is a constant only related to the specific surface area of pores, it indicates the adsorption capacity of coal, so the difference in the adsorption capacity of the experimental coal samples is mainly reflected in the difference in the value of "a"

(2) The process of coal injection into gas is also a process of infiltration and diffusion, percolation is caused by the gas pressure gradient, and diffusion is caused by the concentration gradient [2]. Micropores are the main contributor to the total specific surface area of various pores in coal, providing an excellent place for methane to occur in coal, while medium and large pores provide channels for methane migration. Pore distribution is uneven, and the pores in coal and the connection types between pores are also different. There are interconnected and disconnected pores. The fluid (liquid, methane) in the interconnected pores can pass through, but the pore is not connected to each other; the fluid cannot pass. Porosity is an indicator reflecting the overall development of pores and cracks [17]. The degree of pore and crack development is an important factor that determines the adsorption and permeability of coal. The porosity of a coal sample can be calculated from the true density and apparent density of coal samples. From the results of the analysis on the coal sample methane adsorption process, first, when methane gas molecules enter the coal, they cannot immediately contact all pore surfaces in the coal but form a pressure difference and a concentration difference on the coal sample surface. Under the action of gas pressure difference, the

(a) The seepage process of coal adsorption gas   (b) Schematic diagram of coal matrix gas adsorption
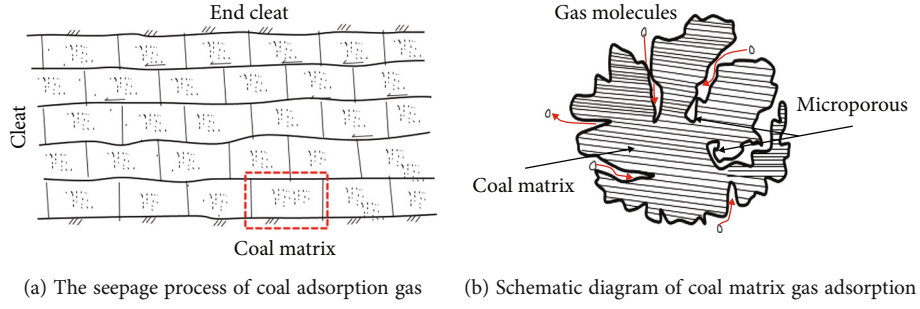
FIGURE 7: Schematic diagram of coal matrix methane adsorption.

methane gas molecules enter the coal sample from the larger pores and cracks on the surface of coal samples; the gas molecules entering the coal sample come into contact with the coal pore surface and adsorb on the pore surface. At the same time, the methane gas molecules are under the action of the concentration difference. It diffuses into the deep pores of the coal sample, and adsorption and desorption occur in the micropores. The gas adsorption process of the coal matrix is shown in Figure 7

Due to the different shapes and degrees of curvature of the coal sample's pores, the path length of the methane molecules that seep into the coal sample is different. The tortuosity factor can be used to measure the degree of curvature of the pores [37], and its physical meaning is the true diffusion distance of methane molecules. The ratio is the apparent diffusion distance. The empirical formula derived by the scholar [38] through theoretical analysis can be used to calculate the tortuosity of the porosity; that is, the tortuosity and porosity parameters of the experimental coal samples are calculated from equations (5) and (6), respectively, and the specific results are shown in Table 3:

$$\tau = \frac{L_t}{L_0}, \tag{4}$$

where τ is tortuosity, L_t the actual distance of the diffusion channel, and L_0 is the straight-line distance of the medium:

$$\varphi = \left(1 - \frac{\rho_s}{\rho_z}\right) \times 100\%, \tag{5}$$

where φ is the porosity (%), ρ_s is the apparent density (g/cm^3), and ρ_z is true density (g/cm^3):

$$\tau = 1 - 0.49 \ln (\varphi). \tag{6}$$

The diffusion of gas in the pores of coal is mainly controlled by micropores; in Figure 3, the pore shapes of coal samples are diverse. In Table 3, the order of the tortuosity of experimental coal samples is WZ>XJ>PDS, indicating that the methane molecules have the longest diffusion path in the WZ coal sample during the same adsorption time, followed by the XJ and PDS coal samples. The WZ coal sample has a large pore specific surface area and can provide

TABLE 3: Porosity and tortuosity parameters of coal samples.

Coal	True density (g·cm^{-3})	Apparent density (g·cm^{-3})	Porosity (%)	Tortuosity
WZ	1.44	1.39	3.47%	2.65
PDS	1.47	1.35	8.16%	2.22
XJ	1.31	1.22	6.87%	2.31

more adsorption sites for the adsorption of tile methane molecules. However, the WZ coal sample methane molecule has a long diffusion channel and greater diffusion resistance during the same charging time, making the amount of methane adsorbed compared to PDS and WZ. Under the same adsorption conditions, due to the different development degrees of coal samples, the pore structure of coal has an impact on the process of methane adsorption.

5. Conclusions

(1) According to the LNA experiment, the proportion of micropore specific surface area of the experimental coal samples is more than 60%, and the ratio of the specific surface area of the micropores increases as the degree of deterioration deepens. Coal sample micropores have a huge internal surface area, which is the main place for gas adsorption. The pore shapes are mostly wedge-shaped holes and ink bottle-shaped pores

(2) Low-field NMR technology provides a new experimental method for coal seam gas flow state to record the dynamic process of gas adsorption. The adsorption conditions are the same, and the relationship between the adsorption and free methane of different experimental coal samples and the aeration time is in the form of a relational formula: $S = abt^c/1 + bt^c$ ($R^2 \geq 0.90$)

(3) The adsorption of gas by coal is mainly related to the coal pore structure. The larger specific surface area of coal samples provides a place for gas adsorption, and the pore types of coal of different grades are different. The porosity and tortuosity of coal samples are different, and the length of methane diffusion channels in coal samples is different. Therefore, the gas

adsorption process of the experimental coal samples is affected by the coal pore structure

(4) This paper only studies the difference in adsorption capacity of experimental coal samples through experiments, and the next step should be to study the control mechanism of the difference in adsorption of different coal ranks from the perspective of molecular models

Data Availability

The underlying data supporting the results of my study can be found in my manuscript.

Conflicts of Interest

The authors declared no potential conflicts of interest with respect to the research, authorship, and/or publication of this article.

Acknowledgments

References

[1] S. N. Zhou and B. Q. Lin, *The Theory of Methane Flow and Storage in Coal Seams*, China coal industry publishing house, Beijing, 1999.

[2] L. Zhang, X. Q. He, and B. S. Nie, "Study on the process of coal absorbing methane," *Mining Safety & Environmental Protection*, vol. 27, no. 6, p. 1-2+4-61, 2000.

[3] S. S. Zhang, H. Liu, Z. H. Jin, and C. Wu, "Multifractal analysis of pore structure in middle- and high-rank coal by mercury intrusion porosimetry and low-pressure N_2 adsorption," *Natural Resources Research*, vol. 30, no. 6, pp. 4565–4584, 2021.

[4] L. J. Sun, *Soft and Hard Coal Adsorption-Desorption Law of Different Coal Rank and It's Application*, China University of Mining and Technology, Beijing, 2013.

[5] Z. W. Li, *Study on Microstructure Characteristics of Low Rank Coal and Its Control Mechanism on Methane Adsorption/ Desorption*, China University of Mining and Technology, 2015.

[6] D. X. Li, E. Y. Wang, X. G. Kong, M. Ali, and D. Wang, "Mechanical behaviors and acoustic emission fractal characteristics of coal specimens with a pre-existing flaw of various inclinations under uniaxial compression," *International Journal of Rock Mechanics and Mining Sciences*, vol. 116, pp. 38–51, 2019.

[7] D. X. Li, E. Y. Wang, Z. H. Li, Y. Ju, D. Wang, and X. Wang, "Experimental investigations of pressure stimulated currents from stressed sandstone used as precursors to rock fracture," *International Journal of Rock Mechanics and Mining Sciences*, vol. 145, article 104841, 2021.

[8] X. L. Li, S. J. Chen, Q. M. Zhang et al., "Research on theory, simulation and measurement of stress behavior under regenerated roof condition," *Geomechanics and Engineering*, vol. 26, no. 1, pp. 49–61, 2021.

[9] X. L. Li, S. J. Chen, S. M. Liu, and Z. H. Li, "AE waveform characteristics of rock mass under uniaxial loading based on Hilbert-Huang transform," *Journal of Central South University*, vol. 28, no. 6, pp. 1843–1856, 2021.

[10] X. Li, S. Chen, and Z. L. EnyuanWang, "Rockburst mechanism in coal rock with structural surface and the microseismic (MS) and electromagnetic radiation (EMR) response," *Engineering Failure Analysis*, vol. 124, no. 6, article 105396, 2021.

[11] W. P. Jiang, X. Z. Song, and L. W. Zhong, "Research on the pore properties of different coal body structure coals and the effects on methane outburst based on the low- temperature nitrogen adsorption method," *Journal of China Coal Society*, vol. 36, no. 4, pp. 609–614, 2011.

[12] X. C. Li, Z. B. Li, L. Zhang et al., "Pore structure characterization of various rank coals and its effect on methane desorption and diffusion," *Journal of China Coal Society*, vol. 44, Supplement 1, pp. 142–156, 2019.

[13] X. L. Li, Z. Y. Cao, and Y. L. Xu, "Characteristics and trends of coal mine safety development," *Part A: Recovery, Utilization, and Environmental Effects*, pp. 1–19, 2020.

[14] J. Y. Jiang, Y. P. Cheng, and S. Zhang, "Quantitative characterization of pore structure and gas adsorption and diffusion properties of low-rank coal," *Journal of China Coal Society*, vol. 46, no. 10, pp. 3221–3233, 2021.

[15] S. M. Liu, X. L. Li, D. K. Wang, and D. Zhang, "Experimental study on temperature response of different ranks of coal to liquid nitrogen soaking," *Natural Resources Research.*, vol. 30, no. 2, pp. 1467–1480, 2021.

[16] L. Qin, P. Wang, S. G. Li et al., "Gas adsorption capacity changes in coals of different ranks after liquid nitrogen freezing," *Fuel*, vol. 292, article 120404, 2021.

[17] Y. B. Yao, D. M. Liu, Y. D. Cai, and J. Q. Li, "Advanced characterization of pores and fractures in coals by nuclear magnetic resonance and X-ray computed tomography," *Chinese Science: Earth Science*, vol. 40, no. 11, pp. 1598–1607, 2010.

[18] X. Chen, T. Yan, F. Zeng, Y. Meng, and J. Liu, "Application of a modified low-field NMR method on methane adsorption of medium-rank coals," *Geofluids*, vol. 2021, 16 pages, 2021.

[19] S. J. Zheng, Y. B. Yao, Y. D. Cai et al., "Characteristics of movable fluid and pore size distribution of low rank coals reservoir in southern margin of Junggar basin," *Coal Geology & Exploration*, vol. 46, no. 1, p. 56-60+65, 2018.

[20] S. B. Xie, Y. B. Yao, J. Y. Cheng et al., "Research of micro-pore structure in coal reservoir using low-field NMR," *Journal of China Coal Society*, vol. 40, Supplement 1, pp. 170–176, 2015.

[21] M. Yang, G. N. Jia, J. L. Gao et al., "Experimental study on the influence of aerated gas pressure and confining pressure on low-rank coal gas adsorption process," *Energy Exploration & Exploitation*, vol. 40, pp. 1–19, 2021.

[22] X. G. Kong, S. G. Li, E. Y. Wang et al., "Experimental and numerical investigations on dynamic mechanical responses and failure process of gas-bearing coal under impact load," *Soil*

Dynamics and Earthquake Engineering, vol. 142, article 106579, 2021.

[23] X. G. Kong, D. He, X. F. Liu et al., "Strain characteristics and energy dissipation laws of gas-bearing coal during impact fracture process," *Energy*, vol. 242, article 123028, 2022.

[24] J. P. Tang, H. N. Tian, N. Yu et al., "Experimental study of influence of gas pressure on coal shale gas adsorption characteristics based on nuclear magnetic resonance spectrum," *Rock and Soil Mechanics*, vol. S2, pp. 203–208, 2016.

[25] Y. B. Yao, D. M. Liu, and S. B. Xie, "Quantitative characterization of methane adsorption on coal using a low-field NMR relaxation method," *International Journal of Coal Geology*, vol. 131, pp. 32–40, 2014.

[26] C. Zheng, D. M. Ma, Y. Chen, Z. Gao, and J. Teng, "Pore structure of different macroscopically distinguished components within low-rank coals and its methane desorption characteristics," *Fuel*, vol. 293, no. 5-6, article 120465, 2021.

[27] F. Yang, D. Ma, Z. Duan, D. Ren, T. Tian, and D. Liu, "Microscopic pore structure characteristics and methane adsorption of vitrain and durain," *Geofluids*, vol. 2020, Article ID 8887230, 18 pages, 2020.

[28] X. R. Sun, *Experimental Research on Pore Structure and Desorption Characteristics of the Low Rank Coal for Fukang Mining Area in Xinjiang*, Xi'an University of Science and Technology, 2015.

[29] K. J. Deng and R. H. Xie, *The Theory and Method of Logging Based on Nuclear Magnetic Resonance*, China University of Petroleum Press, Beijing, 2010.

[30] L. Z. Xiao, *NMR Image Logging and NMR in Rock Experiments*, Science Press, Beijing, 1998.

[31] R. Guo, K. Mannhardt, and A. Kantzas, "Characterizing moisture and gas content of coal by low-field NMR," *Journal of Canadian Petroleum Technology*, vol. 46, no. 10, pp. 49–54, 2007.

[32] S. J. Zheng, Y. B. Yao, D. M. Liu et al., "Quantitative characterization of multiphase methane in coals using the NMR relaxation method," *Journal of Petroleum Science and Engineering*, vol. 198, no. 6, article 108148, 2020.

[33] P. Cheng and X. Y. Tang, "The research on the adsorption of nitrogen in low temperature and micro-pore properties in coal," *Journal of China Coal Society*, vol. 26, no. 5, pp. 552–556, 2001.

[34] C. X. Wang and S. G. Li, "Pore structure characteristics of low rank coal and their influence on methane adsorption," *China Safety Science Journal*, vol. 25, no. 10, pp. 133–138, 2015.

[35] В. В. Ходот, "Coal and methane outburst," in *Translated*, S. Z. Song and Y. A. Wang, Eds., China Industrial Press, Beijing, 1996.

[36] J. J. Zhang, *Pore-Fracture System Characterization and Dynamic Variation of Porosity-Permeability during Multi-Layer Drainage in Middle and High-Rank Coal Reservoirs*, China University of Mining and Technology, Beijing, 2020.

[37] X. Y. Kong, *Advanced Mechanics of Fluids in Porous Media*, University of Science and Technology of China Press, Hefei, 2010.

[38] M. Barrande, R. Bouchet, and R. Denoyel, "Tortuosity of porous particles," *Analytical Chemistry*, vol. 79, no. 23, pp. 9115–9121, 2007.